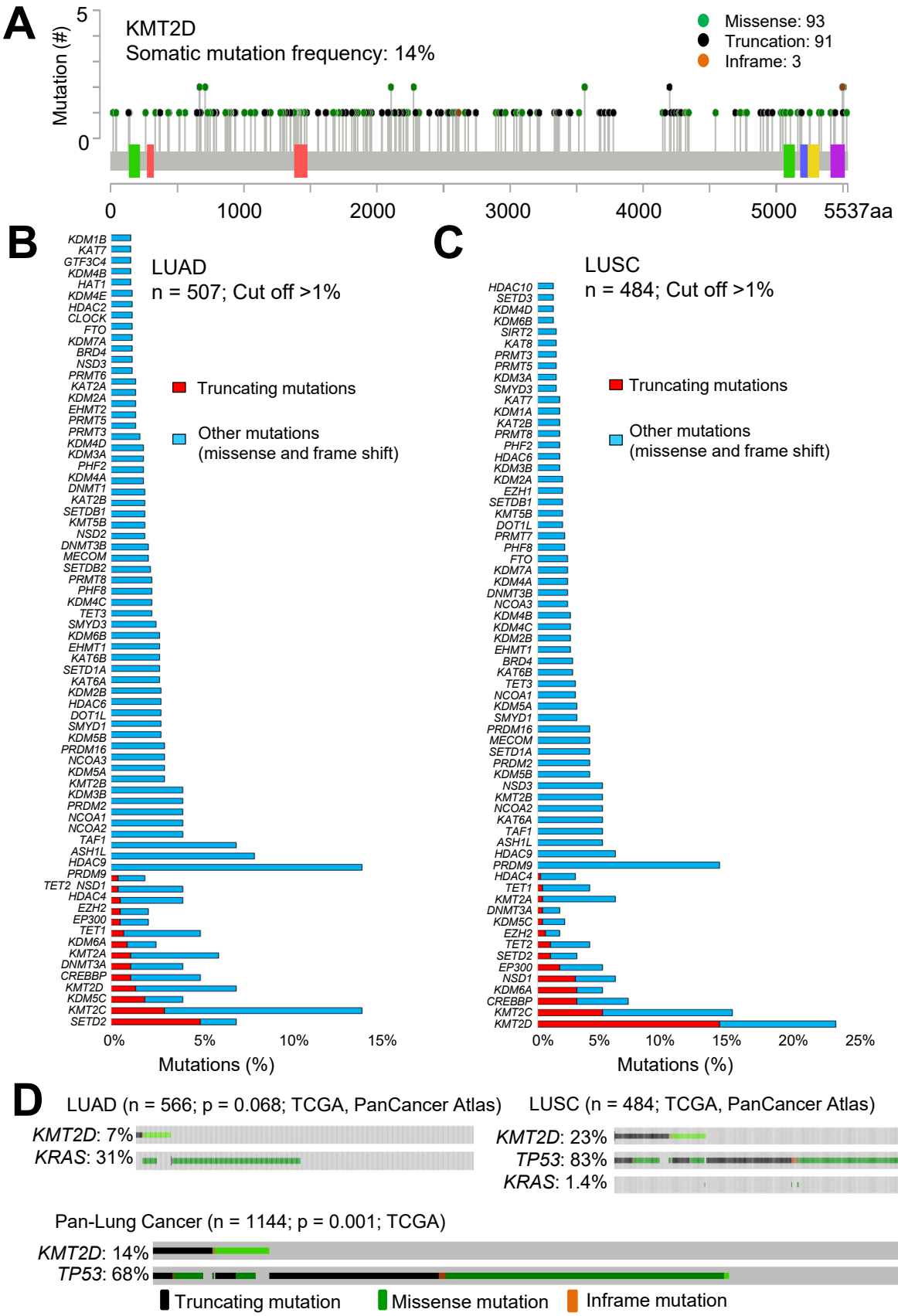

Figure S1, related to **Figure 1.** (**A**) The lollipop graph shows mutation profiles (missense, truncation, and inframe) in the *KMT2D* gene in the Pan-lung cancer TCGA dataset (n = 1144) in the cBioPortal (http://www.cbioportal.org). The percentage of truncating (loss-of-function) mutations in *KMT2D* was 48.7% (91/187). (**B and C**) KMT2D is among the most highly inactivated epigenetic modifiers in human lung cancer. Mutations in epigenetic modifiers in the lung adenocarcinoma (LUAD; n = 507) and lung squamous cell carcinoma (LUSC; n = 484) datasets were analyzed using the cBioPortal. Bar graphs show alterations in epigenetic modifiers containing more than 1% mutations in LUAD (**B**) and LUSC (**C**) samples. Other mutations represent missense and frame shift mutations. (**D**) Analysis of the TCGA LUAD and LUSC dataset in the cBioPortal showed that *KMT2D* mutations often co-occurred with *KRAS* mutations (p = 0.068, Chi-squared test) in human LUAD samples and with *TP53* mutations (p = 0.001, Chi-squared test) in human Pan-lung cancer and LUSC samples. Of the TCGA dataset (n = 1144), *KMT2D*-altered samples and some other samples are shown.

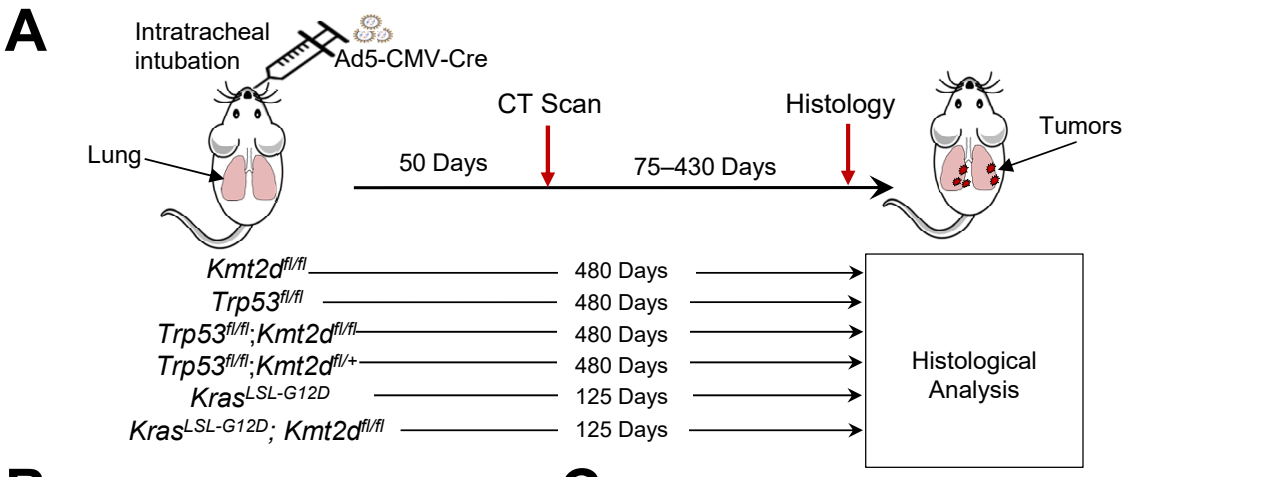

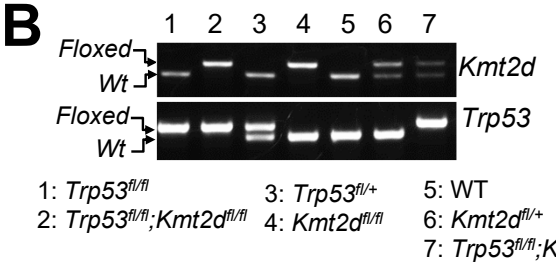

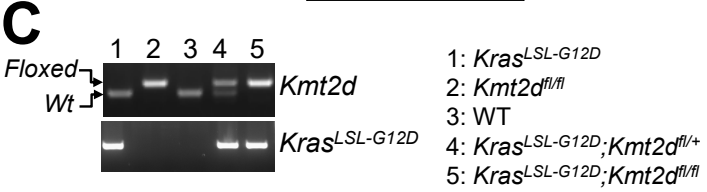

D

Groups	*Kmt2d*$^{fl/fl}$	*Trp53*$^{fl/fl}$	*Trp53*$^{fl/fl}$; *Kmt2d*$^{fl/+}$	*Trp53*$^{fl/fl}$; *Kmt2d*$^{fl/fl}$
Pulmonary adenocarcinomas	0/5 (0%)	0/5 (0%)	0/5 (0%)	0/5 (0%)
Pulmonary adenomas	0/5 (0%)	0/5 (0%)	0/5 (0%)	0/5 (0%)
Multifocal, bronchioloalveolar hyperplasia	0/5 (0%)	0/5 (0%)	0/5 (0%)	0/5 (0%)
BALT hyperplasia	4/5 (80%)	4/5 (80%)	4/5 (80%)	4/5 (80%)

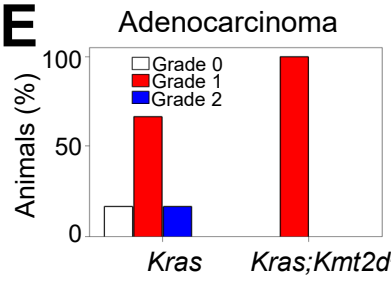

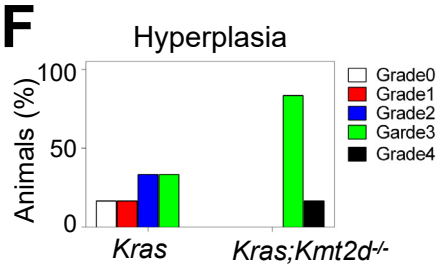

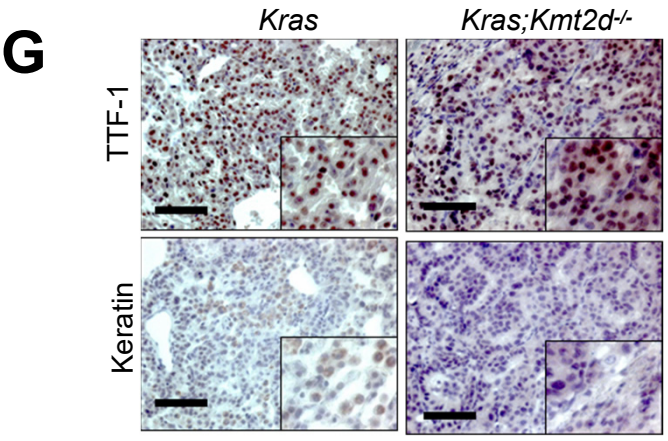

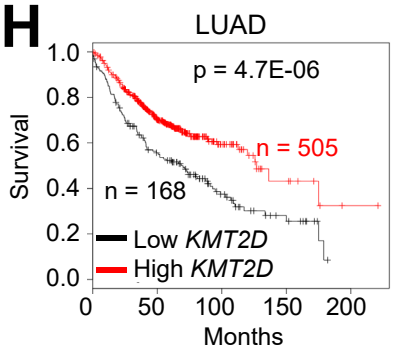

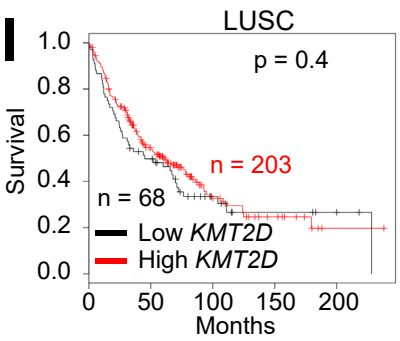

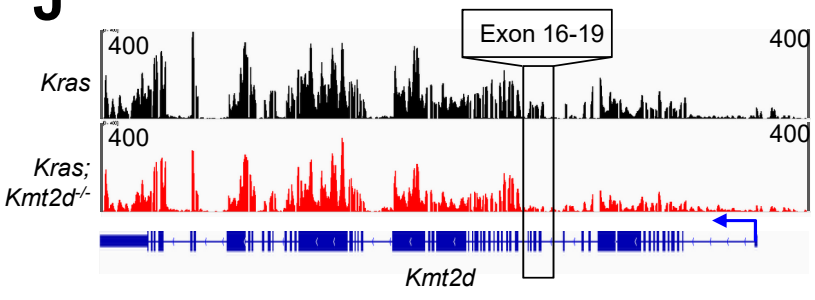

Figure S2, related to **Figure 1**: ***Kmt2d*** **loss accelerates KRAS-driven LUAD tumorigenesis**. (**A**) Our strategy to induce and monitor lung tumorigenesis using new genetically engineered mouse models. (**B** and **C**) Genotyping experiments using specific primers showed the generation of *Trp53*$^{fl/fl}$;*Kmt2d*$^{fl/fl}$ (**B**) and *Kras*$^{LSL\text{-}G12D}$;*Kmt2d*$^{fl/fl}$ (**C**) mice. (**D**) Pulmonary tumors were not observed in lung sections examined microscopically in *Kmt2d*$^{fl/fl}$, *Trp53*$^{fl/fl}$, *Trp53*$^{fl/fl}$;*Kmt2d*$^{fl/+}$, and *Trp53*$^{fl/fl}$;*Kmt2d*$^{fl/fl}$ mice with adeno5 (Ad5)-CMV-Cre mediated gene deletion in the lungs. (**E** and **F**) Microscopic analysis of Ad5-CMV-Cre-infected lungs of *Kras* and *Kras;Kmt2d*$^{-/-}$ mice showed that *Kras;Kmt2d*$^{-/-}$ mice typically had a higher percentage of pulmonary parenchyma effaced by pulmonary adenocarcinoma(s) (**E**) and bronchioloalveolar hyperplasia (**F**) than did *Kras* mice. Tumors and epithelial hyperplasia were graded based on the percentage of the lung effaced by these lesions; higher grades indicate a larger percentage of the pulmonary parenchyma affected. (**G**) Immunohistological (IHC) staining of *Kras* and *Kras;Kmt2d*$^{-/-}$ lung tumors showed that *Kras;Kmt2d*$^{-/-}$ lung tumors, like *Kras* lung tumors, were positive for the lung adenocarcinoma marker TTF-1 and had low levels of the lung squamous carcinoma marker Keratin 5. Scale bars, 100 μm. (**H** and **I**) Kaplan-Meier survival analysis showed that low *KMT2D* mRNA levels correlated with poorer survival in LUAD patients (**H**) but not in LUSC patients (**I**). The KM Plotter database (http://kmplot.com/analysis) was used for this analysis. For LUAD (**H**), the lower quartile was used as a cutoff to divide the samples into *KMT2D*-low (the lowest 25%) and *KMT2D*-high (the remaining 75%) groups. For LUSC (**I**), the auto cut-off function was used to divide samples into low and high KMT2D groups. *KMT2D* probe set, 227527_at. In (**H** and **I**), the statistical analysis was performed using the two-sided log-rank test. (**J**) Genome browser view of normalized signals of RNA-seq data at the *Kmt2d* locus of *Kras* and *Kras;Kmt2d*$^{-/-}$ lung tumor samples showed that *Kras;Kmt2d*$^{-/-}$ mice lost mRNA peaks at exons 16-19. Combined data of two biological replicates from each group are shown.

Table S1, related to **Figure 2**: Gene lists for metabolic pathway, glycolysis, and OXPHOS on the basis of DAVID analysis

Metabolic pathway gene list

1	Sox9	41	Met	81	Prdx3	121	Cox8a	161	Bax	201	Fabp1
2	Fam162a	42	Slc16a3	82	Atp5o	122	Fh1	162	Hadha	202	Nsdhl
3	Chst4	43	Homer1	83	Retsat	123	Ndufb4	163	Mtrr	203	Gpd2
4	Mif	44	Hdlbp	84	Atp5g3	124	Atp1b1	164	Slc25a4	204	Cryz
5	Ak4	45	Cldn9	85	Ndufab1	125	Timm10	165	Ndufc1	205	Aldh9a1
6	Stc2	46	Bpnt1	86	Pdha1	126	Slc25a5	166	Idh3g	206	Ephx1
7	Dsc2	47	Mxi1	87	Timm13	127	Cox5a	167	Abcb7	207	H2afz
8	Tpi1	48	Elf3	88	Mtx2	128	Got2	168	Dld	208	Acads
9	Nt5e	49	Cd44	89	Ndufs6	129	Cyb5r3	169	Ndufa7	209	Abca5
10	Pgk1	50	Srd5a3	90	Maob	130	Gpx4	170	Atp5e	210	Gstk1
11	Sdc1	51	Cited2	91	Etfdh	131	Ndufa1	171	Ugdh	211	Bcar3
12	Egln3	52	Hmmr	92	Ndufa9	132	Cox7a2	172	Ccdc58	212	Ephx2
13	Glrx	53	Mdh2	93	Atp5j2	133	Atp6ap1	173	Pcbd1	213	Rxrg
14	Pcx	54	Sap30	94	Uqcrq	134	Sdhc	174	Suclg2	214	Gc
15	Gfpt1	55	Kif20a	95	Atp6v1e1	135	Decr1	175	Grhpr	215	Paox
16	Ldha	56	Mpi	96	Fxn	136	Timm8b	176	Ywhah	216	Nr3c2
17	Hspa5	57	Gpi1	97	Dlat	137	Aifm1	177	Acsl4	217	Rbp1
18	Eno1	58	Phb2	98	Tomm22	138	Etfa	178	Apex1	218	Pex7
19	Aldh7a1	59	Cycs	99	Atp5c1	139	Acat1	179	Hsd17b11	219	Pex26
20	Gale	60	Mgst3	100	Atp5f1	140	Lrpprc	180	Hsd17b4	220	Nedd4
21	Tsta3	61	Ndufa5	101	Slc25a3	141	Mrpl15	181	Gabarapl1	221	Slc22a18
22	Pfkp	62	Ndufa4	102	Mrpl34	142	Mrpl35	182	Alad	222	Isoc1
23	Hk2	63	Hspa9	103	Vdac2	143	Ndufs7	183	Cbr1	223	Nudt12
24	Sod1	64	Atp5d	104	Ndufb2	144	Atp5j	184	Acsl5		
25	Fkbp4	65	Hsd17b10	105	Pmpca	145	Timm17a	185	Erp29		
26	Pkp2	66	Suclg1	106	Ndufa2	146	Uqcr10	186	Car6		
27	Pygb	67	Cox6a1	107	Uqcrc2	147	Atp5g1	187	Acadl		
28	Slc25a13	68	Atp5b	108	Ndufa3	148	Ndufs8	188	Sms		
29	Hs2st1	69	Vdac1	109	Uqcrh	149	Aco2	189	S100a10		
30	Pgam1	70	Acadm	110	Atp5a1	150	Mrps12	190	Idi1		
31	Gys1	71	Immt	111	Timm50	151	Polr2f	191	Hsd17b7		
32	Me1	72	Uqcr11	112	Atp5g2	152	Atp6v0e	192	Adipor2		
33	Idh1	73	Cox6b1	113	Mrps15	153	Sdha	193	Cpox		
34	P4ha1	74	Cox7c	114	Phyh	154	Por	194	Metap1		
35	Pam	75	Sdhd	115	Afg3l2	155	Grpel1	195	Cbr3		
36	Ak3	76	Cox7a2l	116	Cyc1	156	Cs	196	Ncaph2		
37	Slc37a4	77	Ndufa6	117	Ndufb5	157	Mrps30	197	Ostc		
38	Cdk1	78	Uqcrb	118	Ndufs4	158	Eci1	198	Urod		
39	Rars	79	Atp5h	119	Cox4i1	159	Ndufb6	199	Auh		
40	Mdh1	80	Cox6c	120	Atp6v1f	160	Pdk4	200	D2hgdh		

Table S1, related to **Figure 2**: Continued

Glycolysis gene list

1	Sox9	41	Met
2	Fam162a	42	Slc16a3
3	Chst4	43	Homer1
4	Mif	44	Hdlbp
5	Ak4	45	Cldn9
6	Stc2	46	Bpnt1
7	Dsc2	47	Mxi1
8	Tpi1	48	Elf3
9	Nt5e	49	Cd44
10	Pgk1	50	Srd5a3
11	Sdc1	51	Cited2
12	Egln3	52	Hmmr
13	Glrx	53	Mdh2
14	Pcx	54	Sap30
15	Gfpt1	55	Kif20a
16	Ldha	56	Mpi
17	Hspa5		
18	Eno1		
19	Aldh7a1		
20	Gale		
21	Tsta3		
22	Pfkp		
23	Hk2		
24	Sod1		
25	Fkbp4		
26	Pkp2		
27	Pygb		
28	Slc25a13		
29	Hs2st1		
30	Pgam1		
31	Gys1		
32	Me1		
33	Idh1		
34	P4ha1		
35	Pam		
36	Ak3		
37	Slc37a4		
38	Cdk1		
39	Rars		
40	Mdh1		

OXPHOS gene list

1	Gpi1	41	Uqcrq	81	Atp6ap1
2	Phb2	42	Atp6v1e1	82	Sdhc
3	Cycs	43	Fxn	83	Decr1
4	Mgst3	44	Dlat	84	Timm8b
5	Ldha	45	Tomm22	85	Aifm1
6	Ndufa5	46	Atp5c1	86	Etfa
7	Ndufa4	47	Atp5f1	87	Acat1
8	Hspa9	48	Slc25a3	88	Lrpprc
9	Atp5d	49	Mrpl34	89	Mrpl15
10	Hsd17b10	50	Vdac2	90	Mrpl35
11	Suclg1	51	Ndufb2	91	Ndufs7
12	Cox6a1	52	Pmpca	92	Atp5j
13	Atp5b	53	Ndufa2	93	Timm17a
14	Vdac1	54	Uqcrc2	94	Uqcr10
15	Acadm	55	Ndufa3	95	Atp5g1
16	Immt	56	Uqcrh	96	Ndufs8
17	Uqcr11	57	Mdh2	97	Aco2
18	Cox6b1	58	Atp5a1	98	Mrps12
19	Cox7c	59	Timm50	99	Polr2f
20	Sdhd	60	Atp5g2	100	Atp6v0e
21	Cox7a2l	61	Mrps15	101	Sdha
22	Ndufa6	62	Phyh	102	Por
23	Uqcrb	63	Afg3l2	103	Grpel1
24	Atp5h	64	Cyc1	104	Cs
25	Idh1	65	Ndufb5	105	Mrps30
26	Cox6c	66	Ndufs4	106	Eci1
27	Prdx3	67	Cox4i1	107	Ndufb6
28	Atp5o	68	Atp6v1f	108	Pdk4
29	Retsat	69	Cox8a	109	Bax
30	Atp5g3	70	Fh1	110	Hadha
31	Ndufab1	71	Ndufb4	111	Mtrr
32	Pdha1	72	Atp1b1	112	Slc25a4
33	Timm13	73	Timm10	113	Ndufc1
34	Mtx2	74	Slc25a5	114	Idh3g
35	Mdh1	75	Cox5a	115	Abcb7
36	Ndufs6	76	Got2	116	Dld
37	Maob	77	Cyb5r3	117	Ndufa7
38	Etfdh	78	Gpx4	118	Atp5e
39	Ndufa9	79	Ndufa1		
40	Atp5j2	80	Cox7a2		

Table S2, related to **Figure 2**: Human LUAD samples used for GSEA analysis

TCGA-97-8172-01A	high		TCGA-91-8496-01A	low
TCGA-86-7713-01A	high		TCGA-49-4514-01A	low
TCGA-78-7536-01A	high		TCGA-35-4123-01A	low
TCGA-44-7669-01A	high		TCGA-44-3398-01A	low
TCGA-MP-A4T6-01A	high		TCGA-91-A4BD-01A	low
TCGA-53-7626-01A	high		TCGA-05-5429-01A	low
TCGA-69-8254-01A	high		TCGA-55-6972-01A	low
TCGA-62-8398-01A	high		TCGA-50-5055-01A	low
TCGA-73-4662-01A	high		TCGA-75-5146-01A	low
TCGA-55-8206-01A	high		TCGA-64-5778-01A	low
TCGA-69-8255-01A	high		TCGA-49-4488-01A	low
TCGA-86-8056-01A	high		TCGA-05-5423-01A	low
TCGA-86-7954-01A	high		TCGA-67-3770-01A	low
TCGA-55-A490-01A	high		TCGA-38-4632-01A	low
TCGA-50-5946-01A	high		TCGA-05-5420-01A	low
TCGA-55-7994-01A	high		TCGA-64-1677-01A	low
TCGA-50-5066-02A	high		TCGA-05-5428-01A	low
TCGA-MP-A5C7-01A	high		TCGA-35-5375-01A	low
TCGA-86-7953-01A	high		TCGA-50-5068-01A	low
TCGA-55-7576-01A	high		TCGA-50-5066-01A	low
TCGA-38-4630-01A	high		TCGA-35-4122-01A	truncation mutant
TCGA-97-8171-01A	high		TCGA-69-7979-01A	truncation mutant
TCGA-69-7973-01A	high		TCGA-50-5931-01A	truncation mutant
TCGA-L9-A7SV-01A	high		TCGA-80-5607-01A	truncation mutant

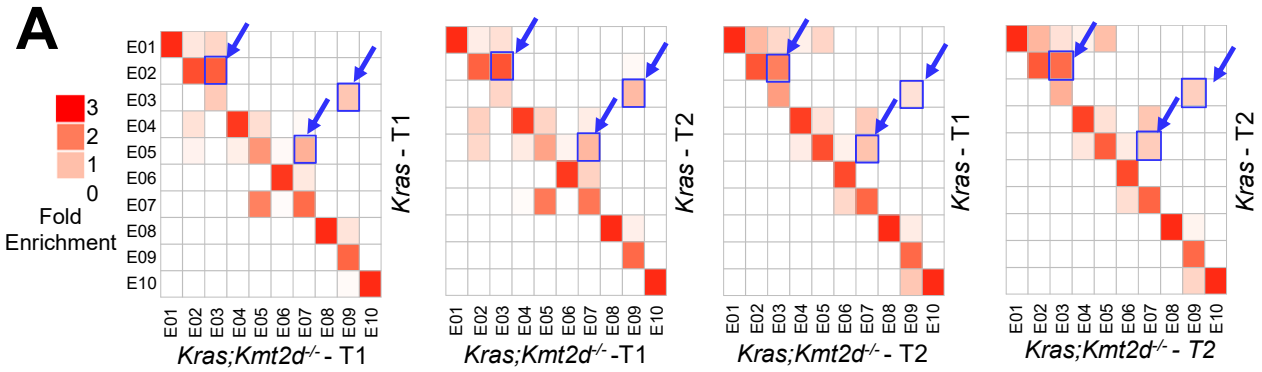
A
Fold Enrichment
3
2
1
0
E01
E02
E03
E04
E05
E06
E07
E08
E09
E10
Kras - T1
Kras - T2
Kras;Kmt2d-/- - T1
Kras;Kmt2d-/- -T1
Kras;Kmt2d-/- - T2
Kras;Kmt2d-/- - T2

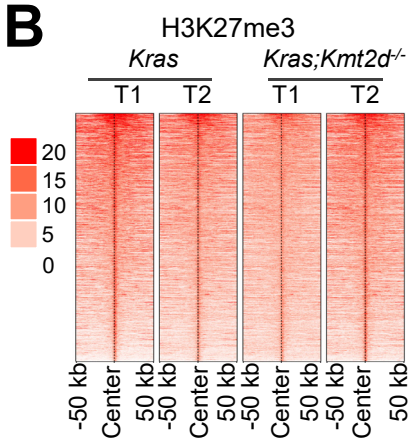
B
H3K27me3
Kras
Kras;Kmt2d-/-
T1
T2
T1
T2
20
15
10
5
0
-50 kb
Center
50 kb

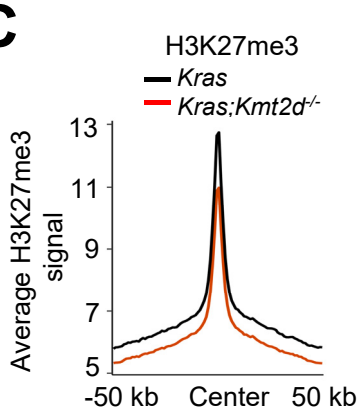
C
H3K27me3
Kras
Kras;Kmt2d-/-
Average H3K27me3 signal
13
11
9
7
5
-50 kb
Center
50 kb

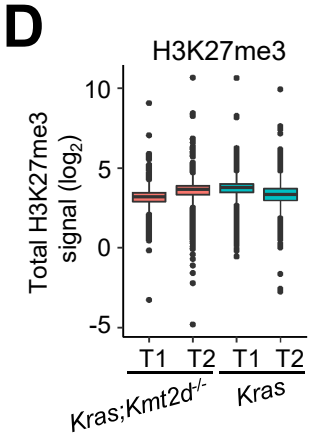
D
H3K27me3
Total H3K27me3 signal (log2)
10
5
0
-5
T1
T2
T1
T2
Kras;Kmt2d-/-
Kras

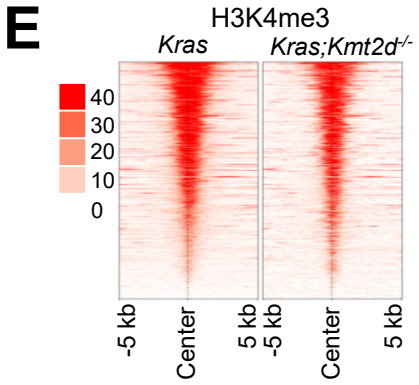
E
H3K4me3
Kras
Kras;Kmt2d-/-
40
30
20
10
0
-5 kb
Center
5 kb

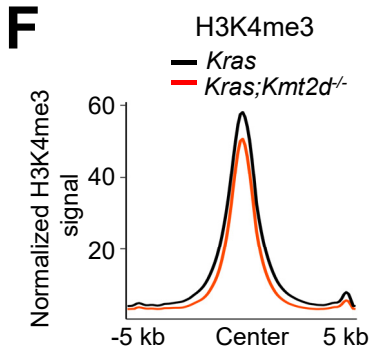
F
H3K4me3
Kras
Kras;Kmt2d-/-
Normalized H3K4me3 signal
60
40
20
-5 kb
Center
5 kb

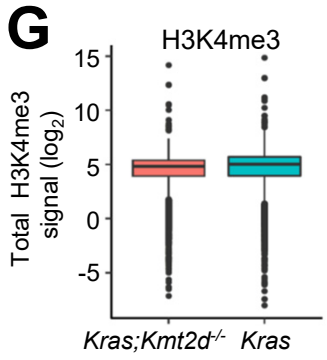
G
H3K4me3
Total H3K4me3 signal (log2)
15
10
5
0
-5
Kras;Kmt2d-/-
Kras

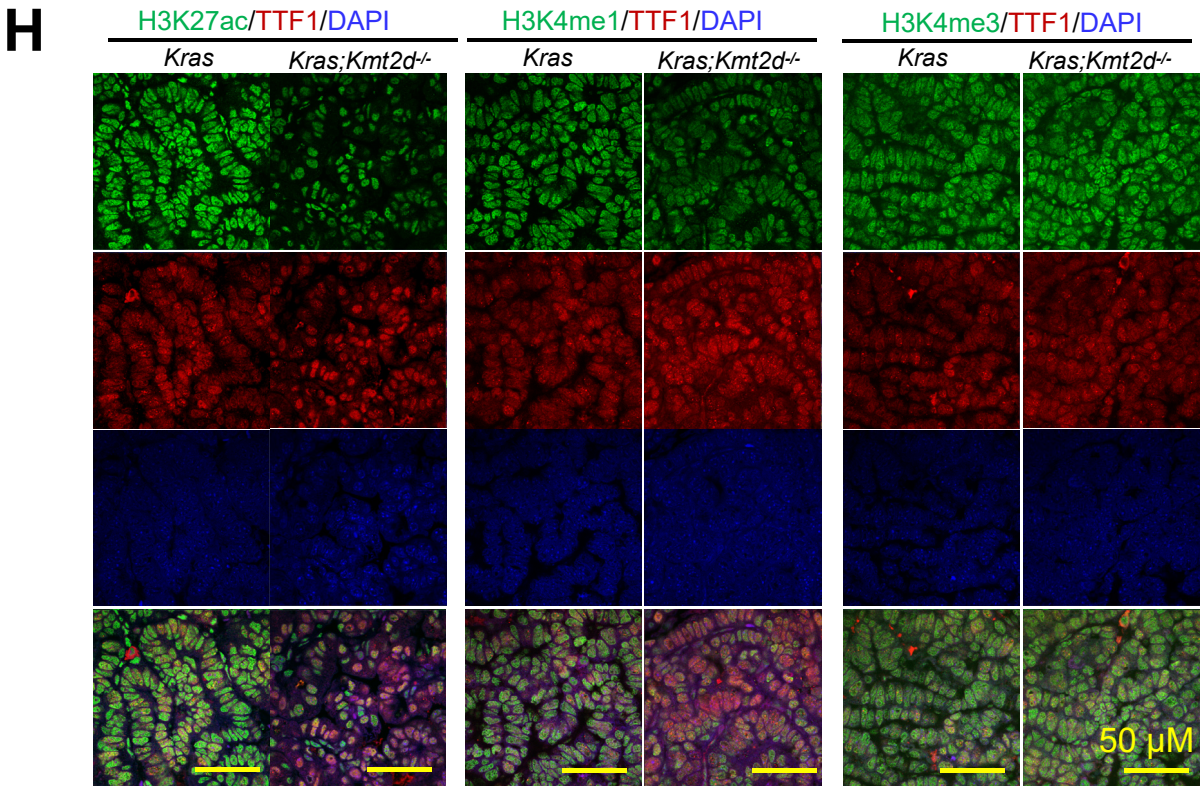
H
H3K27ac/TTF1/DAPI
H3K4me1/TTF1/DAPI
H3K4me3/TTF1/DAPI
Kras
Kras;Kmt2d-/-
50 μM

Figure S3, related to **Figure 4.** (**A**) The comparison between *Kras* and *Kras;Kmt2d*$^{-/-}$ lung tumors revealed three major ChromHMM transitions in chromatin states from *Kras* to *Kras;Kmt2d*$^{-/-}$ lung tumors: E2 (active enhancer) to E3 (weak active enhancer); E3 to E9 (low state = very low signal); and E5 (active enhancer containing low H3K4me1) to E7 (H3K27ac-lacking transcribed enhancer). ChromHMM state transitions in the 10-state ChromHMM model were calculated on the basis of six histone modification profiles between *Kras;Kmt2d*$^{-/-}$ and *Kras* lung tumors. Heat maps show fold enrichment of transitions of chromatin states between *Kras* and *Kras;Kmt2d*$^{-/-}$ lung tumors. The analysis was performed using two different biological replicates. T1, tumor 1; T2, tumor 2. (**B**–**D**) There was no significant difference in global H3K27me3 levels between *Kras* and *Kras;Kmt2d*$^{-/-}$ lung tumors. Heat maps (**B**) and average intensity curves (**C**) of ChIP-Seq reads (RPKM) for H3K27me3 are presented in a 50-kb window centered on the middle of the H3K27me3 peaks in *Kras* and *Kras;Kmt2d*$^{-/-}$ lung tumors. H3K27me3 signals ($\log_2$RPKM) between *Kras* and *Kras;Kmt2d*$^{-/-}$ lung tumors are presented in boxplots (**D**). (**E**–**G**) There was no obvious change in global H3K4me3 levels between *Kras* and *Kras;Kmt2d*$^{-/-}$ lung tumors. Heat maps (**E**) and average intensity curves (**F**) of ChIP-Seq reads (RPKM) for H3K4me3 are presented in a 5-kb window centered on the middle of H3K4me3 peaks in *Kras* and *Kras;Kmt2d*$^{-/-}$ lung tumors. H3K4me3 signals ($\log_2$RPKM) between *Kras* and *Kras;Kmt2d*$^{-/-}$ lung tumors are presented in boxplots (**G**). (**H**) Immunofluorescence staining showed that *Kmt2d* loss downregulated enhancer signals (H3K27ac and H3K4me1) but not H3K4me3 in KRAS-induced mouse lung adenocarcinoma. *Kras* and *Kras;Kmt2d*$^{-/-}$ mouse lung tumor tissues were analyzed. See “Quantification and statistical analysis” in the STAR Method for the description of the boxplots in (**D**) and (**G**). Yellow scale bars, 50 μm.

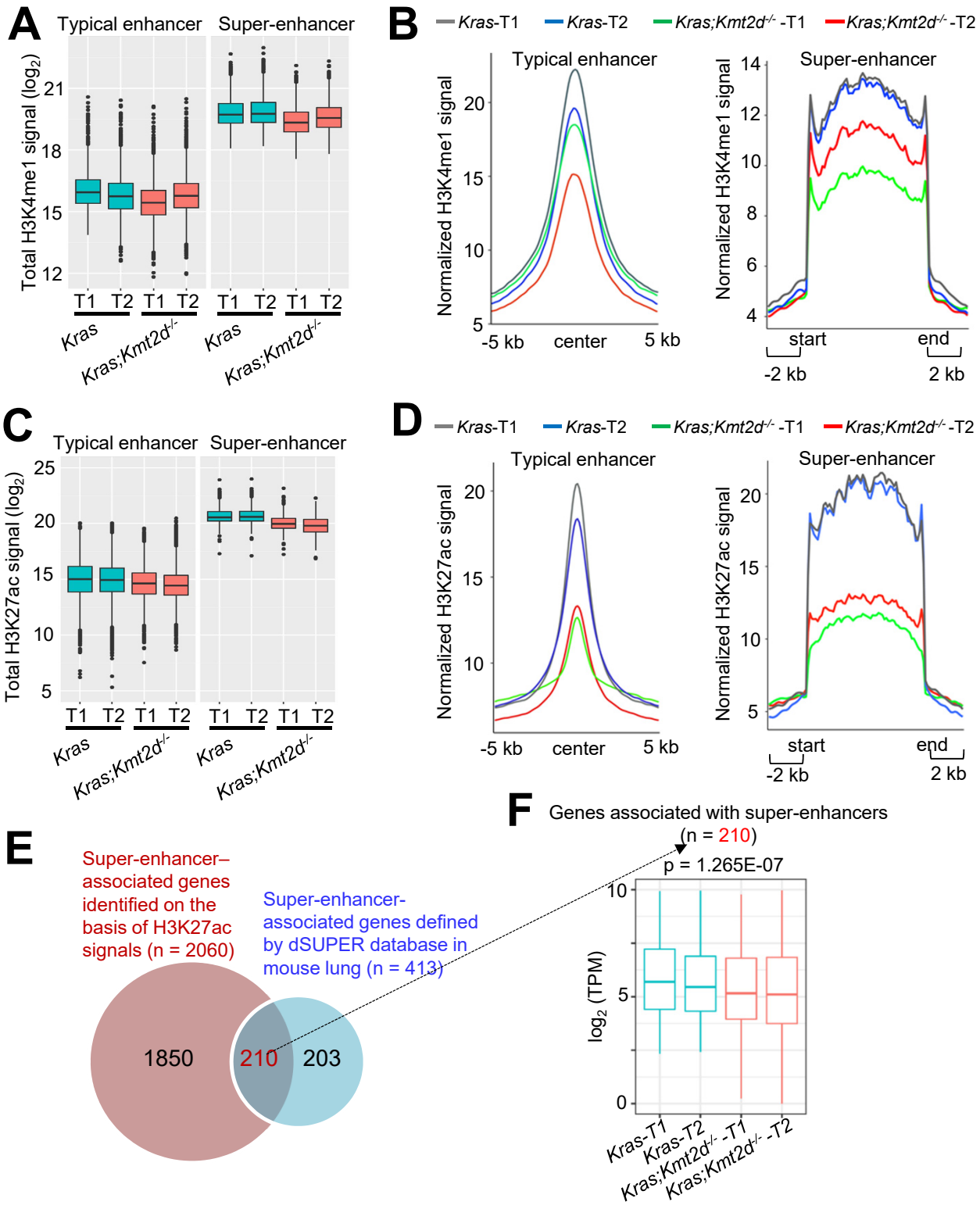

Figure S4, related to **Figure 4**: ***Kmt2d* loss diminishes super-enhancer signals to a greater extent than typical enhancer signals and downregulates expression of lung-enriched, super-enhancer–associated genes in KRAS–induced lung adenocarcinoma.** (**A** and **B**) Analysis of enhancers on the basis of H3K4me1 signals showed that *Kmt2d* loss diminishes more super-enhancers than typical enhancers. Shown are boxplots of H3K4me1 signals for typical enhancers and super-enhancers in *Kras* and *Kras;Kmt2d*$^{-/-}$ lung tumors (**A**). Intensities of ChIP-Seq reads for H3K4me1 at the typical enhancer (left panel) and the super-enhancer (right panel) regions were compared between *Kras* and *Kras;Kmt2d*$^{-/-}$ lung tumors (**B**). (**C** and **D**) Analysis of enhancers on the basis of H3K27ac signals showed that *Kmt2d* loss diminishes more super-enhancers than typical enhancers. Shown are boxplots of H3K27ac signals for typical enhancers and super-enhancers in *Kras* and *Kras;Kmt2d*$^{-/-}$ lung tumors (**C**). Intensities of ChIP-Seq reads for H3K27ac at the typical enhancer (left panel) and super-enhancer (right panel) regions were compared between *Kras* and *Kras;Kmt2d*$^{-/-}$ lung tumors (**D**). (**E**) Venn diagram shows that super-enhancer–associated genes in *Kras* lung tumors substantially overlap with mouse lung super-enhancer genes defined by the dbSUPER database (http://bioinfo.au.tsinghua.edu.cn/dbsuper/). Super-enhancer–associated genes in *Kras* lung tumors were defined on the basis of H3K27ac signals. (**F**) *Kmt2d* loss reduced expression of 210 super-enhancer–associated genes in *Kras* lung tumors. See "Quantification and statistical analysis" in the STAR Method for the description of the boxplots in (**A**), (**C**), and (**F**). T1, Tumor 1; T2, tumor 2.

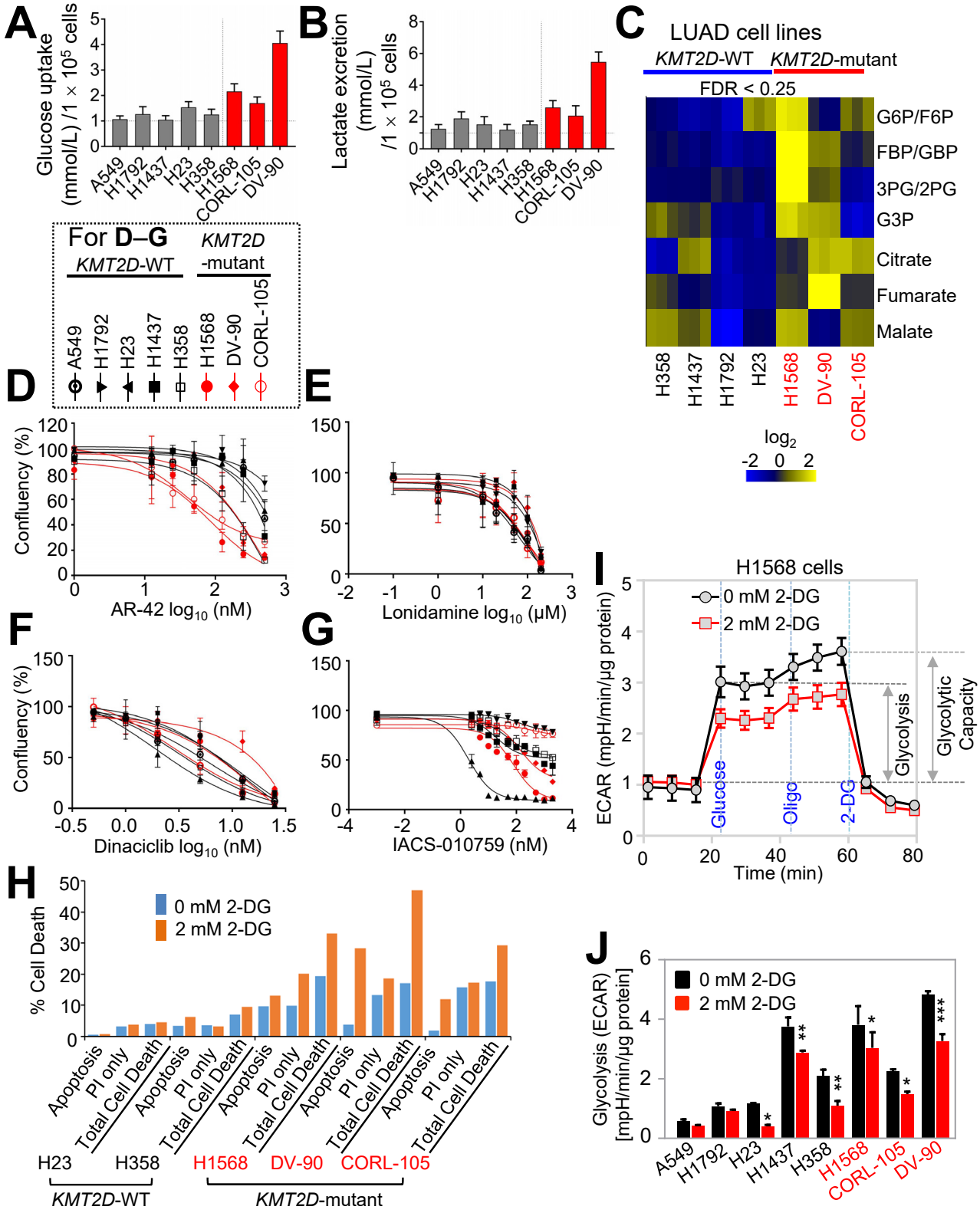

Figure S5, related to **Figure 5**: (**A** and **B**) There were tendencies of higher glucose uptake (**A**) and lactate excretion (**B**) in human LUAD cell lines bearing KMT2D-inactivating mutations (H1568, DV-90 and CORL105) than in human *KMT2D*-WT LUAD cell lines (A459, H1792, H1437, H23, and H358). (**C**) Heatmap showed that some metabolites associated with glycolysis and TCA pathway tended to be upregulated in *KMT2D*-mutant LUAD cell lines (H1568, DV-90 and CORL-105) as compared with *KMT2D*-WT LUAD cell lines (H1437, H23, H1792, and H358). G6P, Glucose-6-phosphate; F6P, Fructose-6-phosphate; GBP, Glucose-1,6-bisphosphate; FBP, Fructose-1,6-bisphosphate; G3P, Glycerol-3-phosphate; 3PG, 3-Phosphoglyceric acid; 2PG, 2-Phosphoglyceric acid; PEP, Phosphoenolpyruvate. (**D–G**) Dose response curves showed that none of AR-42 (**D**), Linodamine (**E**), Dinaciclib (**F**), and IACS-010759 (**G**) selectively inhibited cell confluency of *KMT2D*-mutant LUAD cell lines over *KMT2D*-WT LUAD cell lines. (**H**) Propidium Iodide (PI) staining in combination with FITC-Annexin V staining showed that cell death was largely increased in *KMT2D*-mutant LUAD cell lines as compared with *KMT2D*-WT LUAD cell lines. (**I** and **J**) Metabolic assays using Seahorse showed that 2-DG tended to inhibit ECARs of *KMT2D*-mutant LUAD cell lines to a greater extent than those of *KMT2D*-WT LUAD cell lines. A ECAR graph for H1568 cells is shown (**I**), and ECARs were compared between *KMT2D*-WT and *KMT2D*-mutant LUAD cell lines (**J**). Oligo denotes Oligomycin. *, $p < 0.05$; **, $p < 0.01$; ***, $p < 0.001$ (two-tailed Student's t-test).

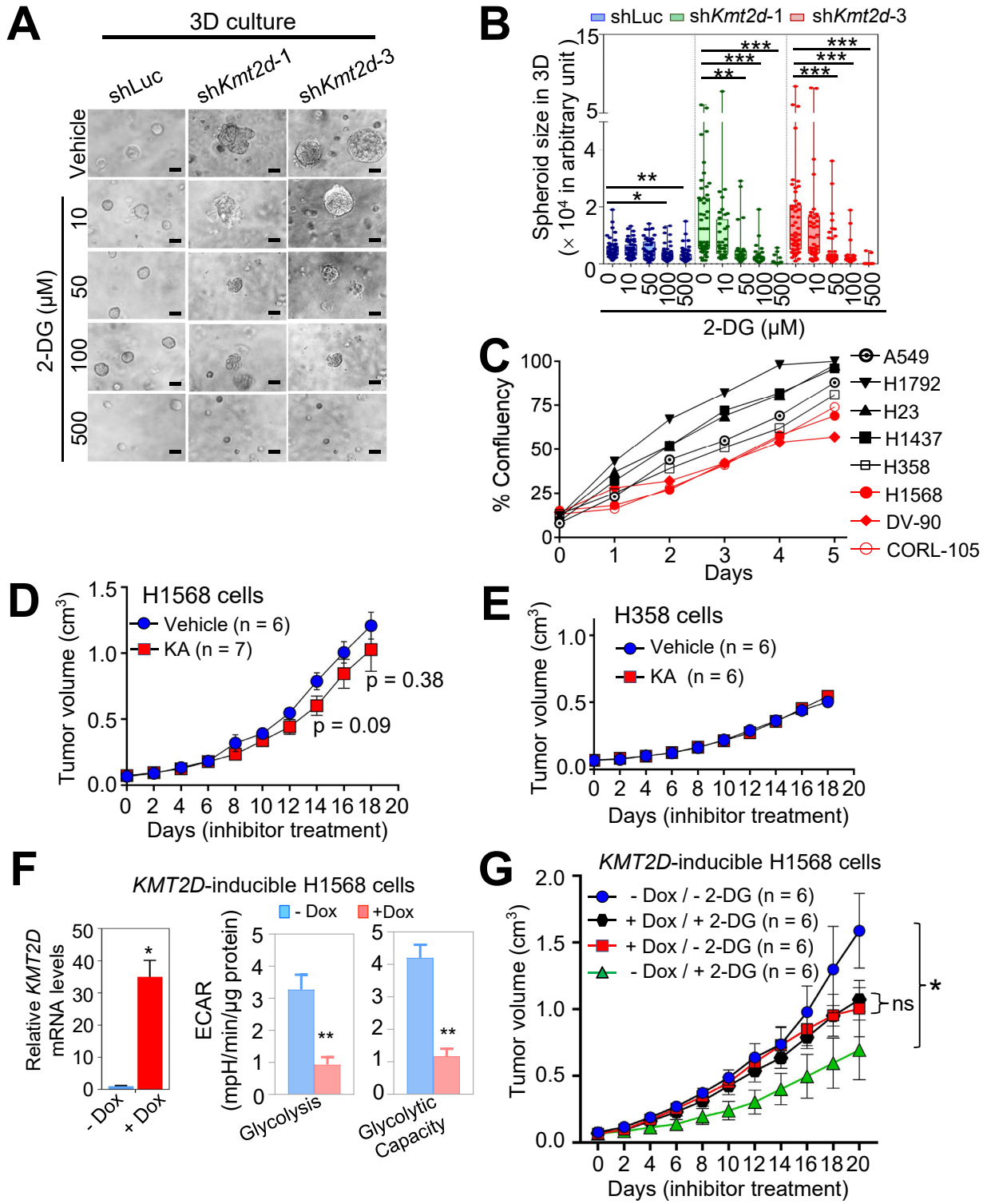

Figure S6, related to **Figure 5**: (**A & B**) Spheroid sizes of LKR-10 cells in a 3D-culture were increased by KMT2D knockdown (sh*Kmt2d*-1 and sh*Kmt2d*-3), and 2-DG treatment inhibited the spheroid growth of KMT2D-depletedLKR-10 cells. Representative images are shown (**A**). The boxplots present the relative sizes of spheroids in 3D-culture (**B**). shLuc-treated cells were used as a control. See "Quantification and statistical analysis" in the STAR Method for the description of the boxplots. Black scale bars, 200 μm. (**C**) The proliferation rates are shown for human *KMT2D*-WT LUAD cell lines (A549, H1792, H23, H1437, and H358) and human *KMT2D*-mutant LUAD cell lines (H1568, DV-90, and CORL105). (**D and E**) Koningic acid (KA) had a weak and insignificant effect on tumorigenic growth of H1568 cells bearing an KMT2D-truncatiing mutation (**D**) while having no effect on tumorigenic growth of H358 cells bearing WT *KMT2D* (**E**) in a mouse subcutaneous xenograft model. The mice were treated with KA (1 mg per kg body weight) every other day for 20 days. (**F**) Doxycycline (Dox)-induced expression of *KMT2D* decreased ECAR in H1568 LUAD cells (Center and right panel). H1568 cells bearing Dox-inducible *KMT2D* were generated, and Dox-induced *KMT2D* mRNA levels were measured (Left panel). Data are presented as the mean ± SEM (error bars) of at least three independent experiments or biological replicates. (**G**) Mouse subcutaneous xenograft results suggested that 2-DG selectively inhibited tumorigenic growth of *KMT2D*-inducible H1568 cells in Dox-untreated mice as compared with Dox-treated mice. Mice were treated with 2-DG (500 mg per kg body weight) or vehicle control every other day for 16 days. For Dox treatment, mice were fed with Dox-containing chow (200 mg Dox per kg of regular mouse chow). *, $p < 0.05$; **, $p < 0.01$; ***, $p < 0.001$ (two-tailed Student's t-test).

Table S3, related to **Figure 5**: Mutation status of the *KMT2D* gene in human lung cancer cell lines

Cell line	Chr	Start Position	End Position	Variant Classification	Variant Type	Reference Allele	Tumor Seq Allele	Protein Change
A549	12	N/A	N/A	N/A				N/A
H1792	12	N/A	N/A	N/A				N/A
H23	12	N/A	N/A	N/A				N/A
H1437	12	N/A	N/A	N/A				N/A
H358	12	N/A	N/A	N/A				N/A
H1568	12	49445194	49445194	Nonsense mutation	SNP	C	A	p.E758*
DV-90	12	49435199	49435199	Frame_Shift_Del	DEL	G	-	p.Pro2118ProfsTer 25(p.P2118fs)
CORL-105	12	49434991	49434991	Frame_Shift_Del	DEL	G	-	p.Arg2188ProfsTer 74(p.R2188fs)

A Characteristics of the top 14 genes

#	Gene	log_2 FC (RNA-seq)	p value (RNA-seq)	log_2 FC (H3K27ac)	p value (H3K27ac)	r (Pearson correlation)	FC_LUAD (Tumor/ Normal)	p value (LUAD)	Survival
1	*SHANK2*	-2.0252	0.005409	-4.28972	4.36E-05	0.49	0.596	***	Low; Poor
2	*MLANA*	-1.74409	0.023769	-1.52758	0.414633	0.33	0.626	***	High; Poor
3	*TRAF3IP1*	-1.54151	0.001934	-1.73023	0.07758	0.42	0.968	Not sig	Low; Poor
4	*ACACB*	-1.16118	7.75E-05	-2.72969	0.003311	0.53	0.312	***	Low; Poor
5	*CRACR2A*	-1.06423	3.95E-04	-2.89113	0.002267	0.3	2.03	***	High; Poor
6	*KIFC3*	-1.04796	9.53E-05	-1.43475	0.062539	0.33	1.03	Not sig	High; Poor
7	*CASZ1*	-0.96877	0.002018	-1.06683	0.156928	0.37	0.459	***	High; Poor
8	*PER2*	-0.92642	0.084606	-1.66447	0.063166	0.35	0.77	***	Low; Poor
9	*NFASC*	-0.89593	0.141034	-2.22851	0.033627	0.3	0.27	***	Low; Poor
10	*CLCN6*	-0.86943	5.63E-04	-2.27149	0.016607	0.48	0.675	***	Low; Poor
11	*TNS2*	-0.852	0.014909	-1.09323	0.129067	0.31	0.326	**	Not sig
12	*ANKRD23*	-0.81188	0.036254	-1.24506	0.252309	0.33	3.11	***	Low; Poor
13	*TMEM2*	-0.79389	0.046892	-1.10537	0.165816	0.33	0.66	***	High; Poor
14	*NAV2*	-0.75495	0.049805	-1.82735	0.0531	0.43	0.983	Not sig	Low; Poor

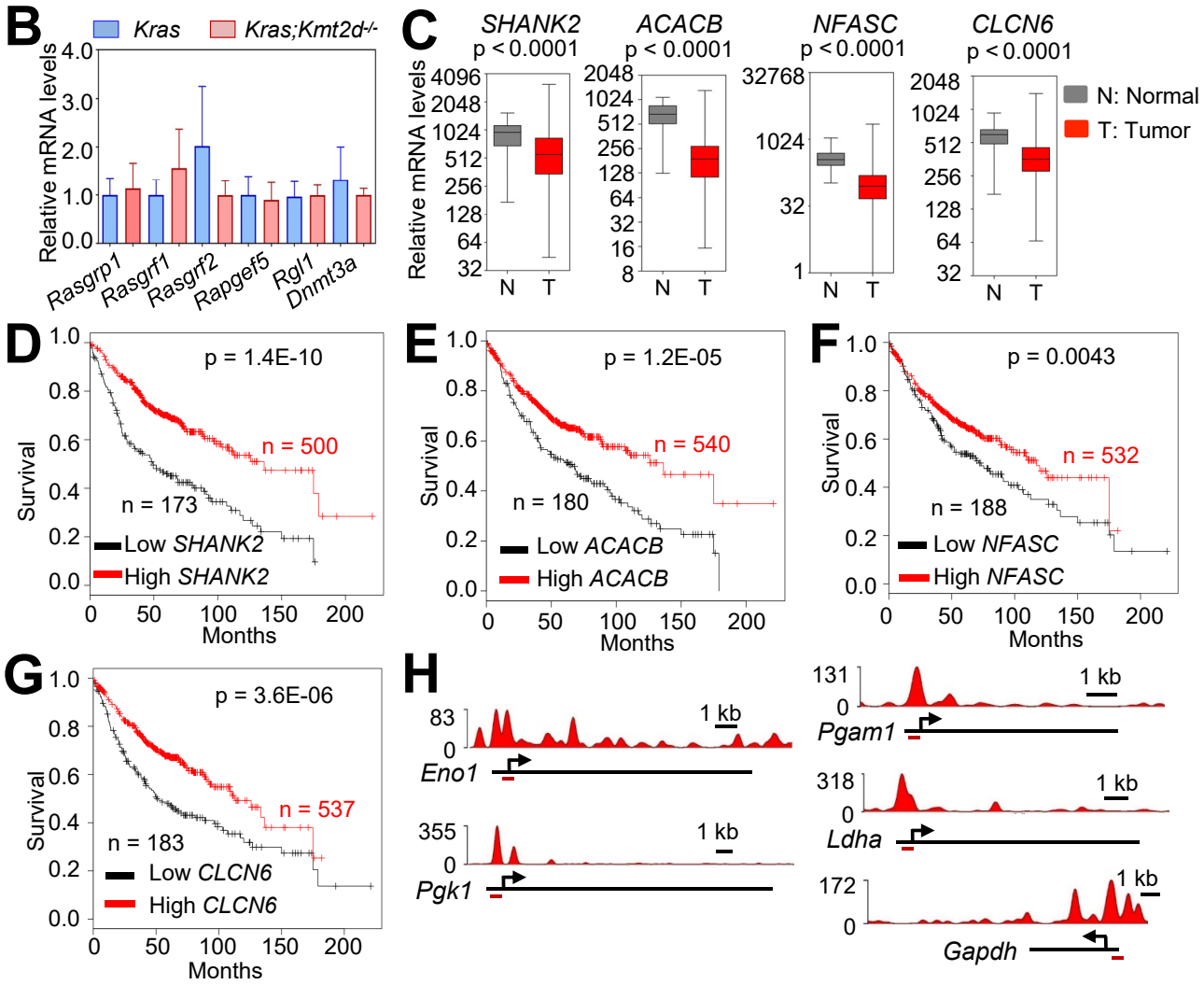

Figure S7, related to **Figures 6 and 7H**: (**A**) Five different characteristics were analyzed for the top 14 genes identified as candidate repressors of glycolysis programs that were upregulated by *Kmt2d* loss. FC, fold change; sig, significant.; **, p < 0.01; ***, p < 0.001 (two-tailed Student's t-test). (**B**) Quantitative RT-PCR results showed that *Kmt2d* loss did not affect expression of *Dnmt3* and Ras activators (*Rasgrp1*, *Rasgrf1*, *Rasgrf2*, *Rapgef5*, and *Rgl1*) in *Kras* tumors. (**C**) *SHANK2*, *ACACB*, *NFASC*, and *CLCN6* mRNA levels were downregulated in lung adenocarcinoma tumor samples (n = 357) as compared with their adjacent normal tissue samples (n = 54) in the TCGA dataset. See "Quantification and statistical analysis" in the STAR Method for the description of the boxplots. (**D–G**) Kaplan-Meier survival analysis using the KM Plotter database (http://kmplot.com/analysis) showed that low *SHANK2* (**D**), *ACACB* (**E**), *NFASC* (**F**), and *CLCN6* (**G**) mRNA levels correlated with worse survival of human lung cancer patients. The lower quartile cutoff was used to divide samples into low and high groups. The statistical analyses were performed using the two-sided log-rank test. *SHANK2,* probe set 243681_at; *ACACB,* probe set 49452_at; *NFASC,* probe set 213438_at; *CLCN6*, probe set 203950_at. (**H**) Our analysis of six sets of public ChIP-seq data (GSM982733, GSM982734, GSM982735, GSM982736, GSM982737, and GSM982738) indicate that PER2 occupied the regions surrounding the transcription start sites. The red bars indicate PCR amplicons (related to **Fig. 7H**).

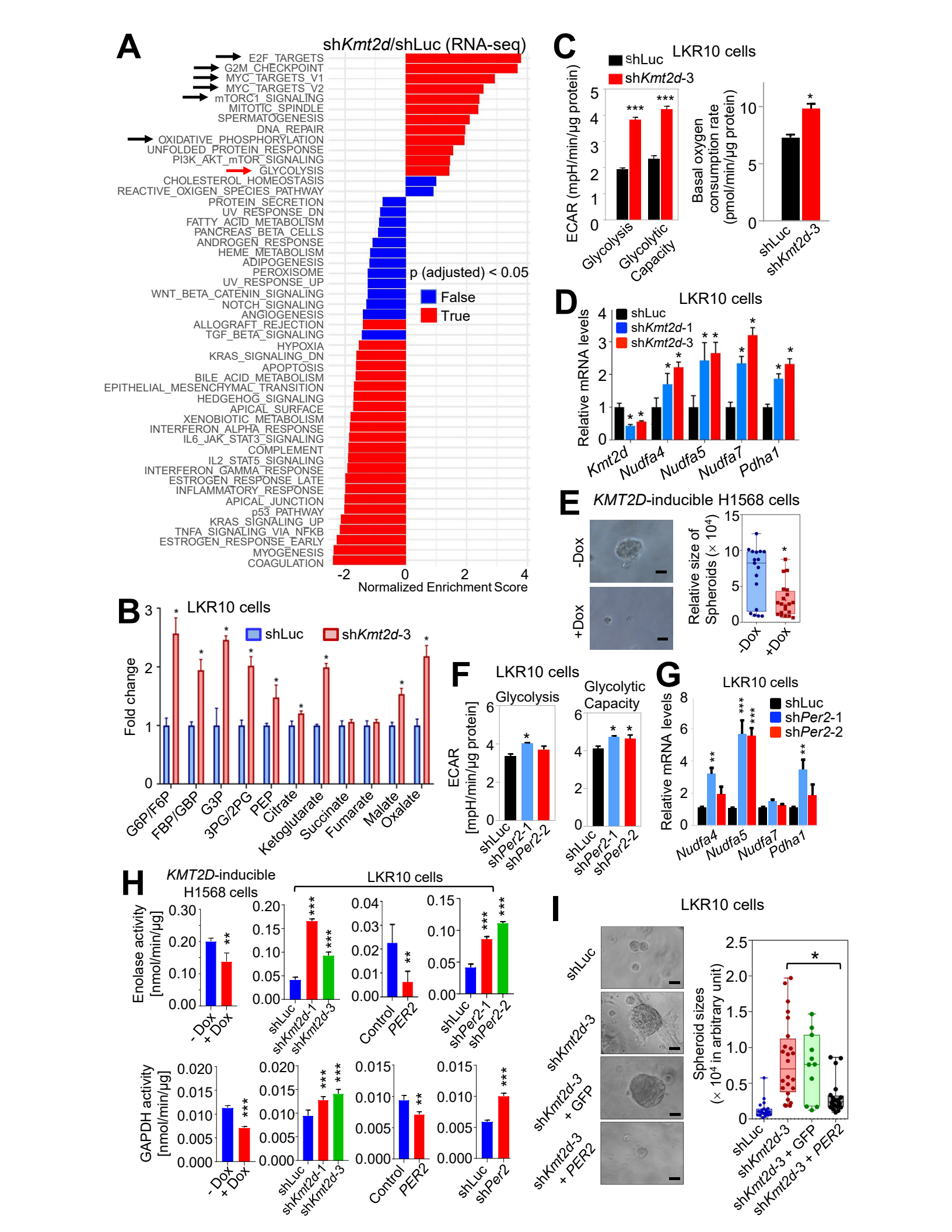
A
shKmt2d/shLuc (RNA-seq)
E2F_TARGETS
G2M_CHECKPOINT
MYC_TARGETS_V1
MYC_TARGETS_V2
mTORC1_SIGNALING
MITOTIC_SPINDLE
SPERMATOGENESIS
DNA_REPAIR
OXIDATIVE_PHOSPHORYLATION
UNFOLDED_PROTEIN_RESPONSE
PI3K_AKT_mTOR_SIGNALING
GLYCOLYSIS
CHOLESTEROL_HOMEOSTASIS
REACTIVE_OXIGEN_SPECIES_PATHWAY
PROTEIN_SECRETION
UV_RESPONSE_DN
FATTY_ACID_METABOLISM
PANCREAS_BETA_CELLS
ANDROGEN_RESPONSE
HEME_METABOLISM
ADIPOGENESIS
PEROXISOME
UV_RESPONSE_UP
WNT_BETA_CATENIN_SIGNALING
NOTCH_SIGNALING
ANGIOGENESIS
ALLOGRAFT_REJECTION
TGF_BETA_SIGNALING
HYPOXIA
KRAS_SIGNALING_DN
APOPTOSIS
BILE_ACID_METABOLISM
EPITHELIAL_MESENCHYMAL_TRANSITION
HEDGEHOG_SIGNALING
APICAL_SURFACE
XENOBIOTIC_METABOLISM
INTERFERON_ALPHA_RESPONSE
IL6_JAK_STAT3_SIGNALING
COMPLEMENT
IL2_STAT5_SIGNALING
INTERFERON_GAMMA_RESPONSE
ESTROGEN_RESPONSE_LATE
INFLAMMATORY_RESPONSE
APICAL_JUNCTION
p53_PATHWAY
KRAS_SIGNALING_UP
TNFA_SIGNALING_VIA_NFKB
ESTROGEN_RESPONSE_EARLY
MYOGENESIS
COAGULATION
p (adjusted) < 0.05
False
True
-2
0
2
4
Normalized Enrichment Score
B
LKR10 cells
shLuc
shKmt2d-3
Fold change
G6P/F6P
FBP/GBP
G3P
3PG/2PG
PEP
Citrate
Ketoglutarate
Succinate
Fumarate
Malate
Oxalate
C
LKR10 cells
shLuc
shKmt2d-3
ECAR (mpH/min/μg protein)
Glycolysis
Glycolytic Capacity
Basal oxygen consumption rate (pmol/min/μg protein)
shLuc
shKmt2d-3
D
LKR10 cells
shLuc
shKmt2d-1
shKmt2d-3
Relative mRNA levels
Kmt2d
Nudfa4
Nudfa5
Nudfa7
Pdha1
E
KMT2D-inducible H1568 cells
-Dox
+Dox
Relative size of Spheroids (× 10⁴)
-Dox
+Dox
F
LKR10 cells
Glycolysis
Glycolytic Capacity
ECAR [mpH/min/μg protein]
shLuc
shPer2-1
shPer2-2
G
LKR10 cells
shLuc
shPer2-1
shPer2-2
Relative mRNA levels
Nudfa4
Nudfa5
Nudfa7
Pdha1
H
KMT2D-inducible H1568 cells
LKR10 cells
Enolase activity [nmol/min/μg]
- Dox
+ Dox
shLuc
shKmt2d-1
shKmt2d-3
Control
PER2
shLuc
shPer2-1
shPer2-2
GAPDH activity [nmol/min/μg]
- Dox
+ Dox
shLuc
shKmt2d-1
shKmt2d-3
Control
PER2
shLuc
shPer2
I
LKR10 cells
shLuc
shKmt2d-3
shKmt2d-3 + GFP
shKmt2d-3 + PER2
Spheroid sizes (× 10⁴ in arbitrary unit)
shLuc
shKmt2d-3
shKmt2d-3 + GFP
shKmt2d-3 + PER2

Figure S8: related to **Figure 8.**

(**A**) GSEA analysis of RNA-seq data showed that KMT2D knockdown increased tumor-promoting programs, such as glycolysis, OXPHOS, E2F targets, and MYC targets, in mouse LKR10 cells. sh*Kmt2d* represents a combination of two RNA-seq datasets of sh*Kmt2d*-1-treated cells and two RNA-seq datasets of sh*Kmt2d*-3-treated cells. shLuc (shLuciferase) indicates a combination of two RNA-seq datasets of shLuc-treated cells. The MsigDB Gene Set was used as a reference. (**B**) Mass spectrometric analysis of metabolomics showed that KMT2D knockdown upregulated many glycolysis metabolites and certain TCA metabolites in mouse LKR-10 cells. G6P, Glucose-6-phosphate; F6P, Fructose-6-phosphate; GBP, Glucose-1,6-bisphosphate; FBP, Fructose-1,6-bisphosphate; G3P, Glycerol-3-phosphate; 3PG, 3-Phosphoglyceric acid; 2PG, 2-Phosphoglyceric acid; PEP, Phosphoenolpyruvate. (**C**) Metabolic assays using Seahorse showed that KMT2D knockdown in LKR10 cells increased ECAR but slightly augmented oxygen consumption rate. (**D**) Quantitative RT-PCR analysis demonstrated that KMT2D knockdown increased expression of the OXPHOS genes *Ndufa4*, *Ndufa5*, *Ndufa7*, and *Pdha1* in mouse LKR-10 cells. (**E**) Dox-induced expression of *KMT2D* decreased spheroid sizes of H1568 cells bearing an KMT2D-inactivating mutation in a 3D culture. Representative images of spheroids are shown (left panel). The sizes of the spheroids were quantified (right panel). Dox-untreated cells were used as a control. Dox was used in a concentration of 10 μg/ml. Black scale bars, 200 μm. (**F** & **G**) PER2 knockdown increased ECARs (**F**) and expression of certain OXPHOS genes (**G**) in LKR10 cells. (**H**) Enzyme assays showed that KMT2D or PER2 knockdown upregulated ENO1 and GAPDH activities in LKR10 cells whereas *KMT2D* or *PER2* overexpression reduced their activities in H1568 cells or LKR10 cells, respectively. The expression plasmid pLenti-*PER2* was used for *PER2* overexpression. (**I**) Exogenous *PER2* expression reduced spheroid sizes of KMT2D-depleted LKR-10 cells in a 3D-culture. Representative images of spheroids are shown (left panel). The sizes of the spheroids were quantified (right panel). shLuc and pLenti-GFP viruses were used as controls. Black scale bars represent 200 μm. In (**B**–**D**) and (**F**–**H**), data are presented as the mean ± SEM (error bars) of at least three independent experiments or biological replicates. See “Quantification and statistical analysis” in the STAR Method for the description of the boxplots in **E** and **I**. *, $p < 0.05$; **, $p < 0.01$; ***, $p < 0.001$ (two-tailed Student’s t-test).

Table S4, related to **STAR Methods**: Oligonucleotides

Oligonucleotides				
Primers for quantitative RT-PCR (mouse)				
Gene		Sequence	Source	IDENTIFIER
Kmt2d	F	GGC GTT GTG TGG AGT GTA TC	Integrated DNA Technologies	N/A
	R	CAC AGT CAT CAC AGA GCA GC		
Eno1	F	CAT GGG GAA GGG TGT CTC AC	Integrated DNA Technologies	N/A
	R	GTG CCG TCC ATC TCG ATC AT		
Pgk1	F	ATG TCG CTT TCC AAC AAG CTG	Integrated DNA Technologies	N/A
	R	GCT CCA TTG TCC AAG CAG AAT		
Pgam1	F	TCT GTG CAG AAG AGA GCA ATC C	Integrated DNA Technologies	N/A
	R	CTG TCA GAC CGC CAT AGT GT		
Gapdh	F	CATGGCCTTCCGTGTTCCTA	Integrated DNA Technologies	N/A
	R	GCCTGCTTCACCACCTTCTT		
Ldha	F	ACC TCG GTA TTA TTT TTC CAT TTC A	Integrated DNA Technologies	N/A
	R	TGT AAT CTT GTT CTG GGG AGC C		
Per2	F	GAA AGC TGT CAC CAC CAT AGA A	Integrated DNA Technologies	N/A
	R	AAC TCG CAC TTC CTT TTC AGG		
Cdk1	F	AGA AGG TAC TTA CGG TGT GGT	Integrated DNA Technologies	N/A
	R	GAG AGA TTT CCC GAA TTG CAG T		
Ndufa4	F	CGG CTT AGC GTG TGT CCT AA	Integrated DNA Technologies	N/A
	R	GCC AAG CGC ATC ACA TAC AG		
Ndufa5	F	GAT TGA GCG GGC TTG GGA AA	Integrated DNA Technologies	N/A
	R	AAC ATC TGG CTC CTC GTG TG		
Ndufa7	F	CCGCTACTCGCGTTATCCAA	Integrated DNA Technologies	N/A
	R	TTGGACAGCTTGTGACTGGG		
Pdha	F	GCA AAC TTG AAG CCA GCC ATC	Integrated DNA Technologies	N/A
	R	TCC ACA CCT CTA CAC AGA GC		
Gpi1	F	TGG CAA ATC CAT CAC GGA CA	Integrated DNA Technologies	N/A
	R	GGA AGT CTC AGG GGA CAA GC		
Actin	F	GGC TGT ATT CCC CTC CAT CG	Integrated DNA Technologies	N/A
	R	CCA GTT GGT AAC AAT GCC ATG T		
18S	F	TAGAGGGACAAGTGGCGTTC	Integrated DNA Technologies	N/A
	R	CGCTGAGCCAGTCAGTGT		
Primers for quantitative RT-PCR for enhancer RNAs				
Per2-E1	F	GTG GGT CCA ACC TCT CCA AG	Integrated DNA Technologies	N/A
	R	ATG CTC GCC ATC CAC AAG AA		
Per2-E2	F	CAA CTG TTT GCC TCT TGC CC	Integrated DNA Technologies	N/A
	R	GAG CTG GCT TCC CTT CTC AG		
Primers for genotyping				
$Kmt2d^{fl/fl}$	F	AGAATGGACACTGGAGCTCC	Integrated DNA Technologies	N/A
	R	AGAAATCCCCAACCACAGC		
$Trp53^{fl/fl}$	F	GGT TAA ACC CAG CTT GAC CA	Integrated DNA Technologies	N/A
	R	GGA GGC AGA GAC AGT TGG AG		
$Kras^{LSL-G12D}$	F	CTA GCC ACC ATG GCT TGA GT	Integrated DNA Technologies	N/A
	R	TCC GAA TTC AGT GAC TAC AGA TG		
Primers for quantitative ChIP-PCR (mouse)				
Per2-A	F	AGC AGG GTC ATG TTG AGC ATT C		N/A

	R	AGG TTC TTG CCA TGA AGA AGG TA	Integrated DNA Technologies	
Per2-B	F	GGT GCA CAT CCA TAG AAC TGA GA	Integrated DNA Technologies	N/A
	R	TGA ATG TCA TGA GTC CCT CAG C		
Per2-C	F	ATT GAC GGC AAT GGT GGC TA	Integrated DNA Technologies	N/A
	R	TGC AGG CCA AAT GTA GAG CA		
Per2-D	F	CTCCCGTCATTTCCTCTTCAC	Integrated DNA Technologies	N/A
	R	GTTAAGGAGCCAGAGACACAAG		
Eno1	F	TAA CGA GCA GGA AAG GAA GAC	Integrated DNA Technologies	N/A
	R	AGG AGA GCC TTA AGG ACA GA		
Pgk1	F	CAA CCG GCT CCG TTC TTT	Integrated DNA Technologies	N/A
	R	GTG AGA CGT GCT ACT TCC ATT T		
Pgam1	F	GTG GCA GAG ACA GGA AAT CT	Integrated DNA Technologies	N/A
	R	GAC AGT CTC TCT GCG TAA CC		
Ldha	F	GCG GAG GAT CGA TGC ATT TC	Integrated DNA Technologies	N/A
	R	ACG ATG TCC CTG CAA GAG T		
Gapdh			Active motif	Cat#: 71018
Primers for cloning				
MLL4 into pInducer 20	F	GGGGACAACTTTGTACAAAAAAGTTGGCatggacagccagaagctg	Integrated DNA Technologies	N/A
	R	GGGGACAACTTTGTACAAGAAAGTTGGGgttcatccatttccgacaattc		